How to cite: *Angew. Chem. Int. Ed.* **2025**, *64*, e202422075
doi.org/10.1002/anie.202422075

Peptide Nanostructures | Hot Paper

Beyond Dimerization: Harnessing Tetrameric Coiled-Coils for Nanostructure Assembly

*Sara Vidmar[+], Tamara Šmidlehner[+], Jana Aupič, Žiga Strmšek, Ajasja Ljubetič, Fei Xiao, Guang Hu, Chuan Liu, Florian Beck, Philipp S. Erdmann, and Roman Jerala**

Abstract: Versatile DNA and polypeptide-based structures have been designed based on complementary modules. However, polypeptides can also form higher oligomeric states. We investigated the introduction of tetrameric modules as a substitute for coiled-coil dimerization units used in previous modular nanostructures. Tetramerizing helical bundles can run in parallel or antiparallel orientation, expanding the number of topological solutions for modular nanostructures. Furthermore, this strategy facilitates the construction of nanostructures from two identical polypeptide chains. Importantly, tetrameric modules substantially stabilized protein nanostructures against air–water interface denaturation, enabling the determination of the first cryo-electron microscopy three-dimensional structure of a coiled-coil-based nanostructure, confirming the designed agreement of the modules forming a tetrahedral cage.

Introduction

Several design principles have emerged to construct programmable nanostructures composed of nucleic acids or polypeptides. DNA nanotechnology has demonstrated the potential of modular design principles, using programmable complementary pairing modules to build complex assemblies.[1–5] A similar pairwise complementarity has been applied to polypeptide nanostructures based on dimeric coiled coils, called coiled-coil protein origami (CCPO) mimicking DNA strand complementarity. We have shown that different polypeptide assemblies, such as tetrahedrons,[6,7] four-sided pyramids, triangular prisms, and trigonal bipyramids[8] can fold in mammalian cells and in vivo.[6] Pre-organized modules also enabled the formation of an octahedral cage.[8,9] The underlying building modules of CCPO were coiled-coil dimers (CC), supramolecular building blocks that consist of two α-helices wrapped around each other in either parallel or antiparallel orientation.[10,11] The dimeric coiled-coil assembly is defined by the network of electrostatic and hydrophobic interactions originating from amino acids positioned at **a**, **d**, and **e**, **g** sites within the heptad repeat.[10,12,13] Orthogonal pairs were precisely arranged within the polypeptide chain to self-assemble into dimeric modules, driving the self-assembly process and forming the edges of polyhedra as in DNA nanostructures.[11] The design of CC-based nanostructures follows a topological path that traverses each edge of the polyhedral precisely twice.[7] Thus, six pairs of orthogonal dimeric CCs arranged in a defined order are required to construct a tetrahedron. To reduce the number of unique coiled-coil pairs needed, we recently demonstrated that by designing the sequential order of CCs to avoid mispairing, multiple copies of the same module can be incorporated in the same chain while maintaining the properly folded

[*] S. Vidmar,[+] T. Šmidlehner,[+] J. Aupič, Ž. Strmšek, A. Ljubetič, R. Jerala
Department of Synthetic Biology and Immunology
National Institute of Chemistry
Ljubljana, Slovenia
E-mail: roman.jerala@ki.si

A. Ljubetič, R. Jerala
EN-FIST Centre of Excellence
Ljubljana, Slovenia

S. Vidmar[+]
Interdisciplinary Doctoral Programme in Biomedicine
University of Ljubljana
Ljubljana, Slovenia

F. Xiao, G. Hu
MOE Key Laboratory of Geriatric Diseases and Immunology
Suzhou Key Laboratory of Pathogen Bioscience and Anti-infective Medicine
Department of Bioinformatics, Center for Systems Biology, School of Life Sciences
Suzhou Medical College of Soochow University
Suzhou, China

C. Liu, P. S. Erdmann
Human Technopole
Milan, Italy

C. Liu, F. Beck
Department of Molecular Structural Biology
Max Planck Institute of Biochemistry
Martinsried, Germany

[+] contributed equally

geometry.[14] Self-assembling oligomeric nanocages have been reported, composed of a handful to several hundred protomers.[15–19] Protein nanocages compromising an inner cavity are particularly interesting as they could be used as delivery systems and for compartmentalization.

The modular CCPO cages reported so far are based on coiled-coil dimers, similar to DNA pairing. However, polypeptides may also engage in other interactions, which could be used as modules. Here, we present the expansion of modularly designed nanostructures, where instead of relying solely on dimeric CCs as building blocks, we introduce tetrameric coiled coils to form tetrahedral assemblies. This new approach expands the number of possible polypeptide chain topologies and enables tuning the properties of protein nanocages, such as their rigidity and stability. Moreover, polypeptide-based tetramers are available in parallel or antiparallel organizations, which expands the number of diverse designs. Additionally, by introducing homo-tetrameric parallel building blocks, we can design homodimeric protein cages with, e.g., tetrahedral topologies, that are virtually identical to their single-chain analogs but reduce the required polypeptide chain length in half. We show that CCPO cages compromising tetrameric modules are more resistant to air–water interface denaturation than solely CC-dimer-based designs and facilitate structure determination using cryo-electron microscopy. We confirm the success of designs and their properties by molecular dynamics (MD) simulations, small angle X-ray scattering (SAXS), and a single particle cryo-EM structure of one of the tetrahedral nanocages, which confirms the protein fold, the position of a four helical bundle module, and the pronounced inner cavity.

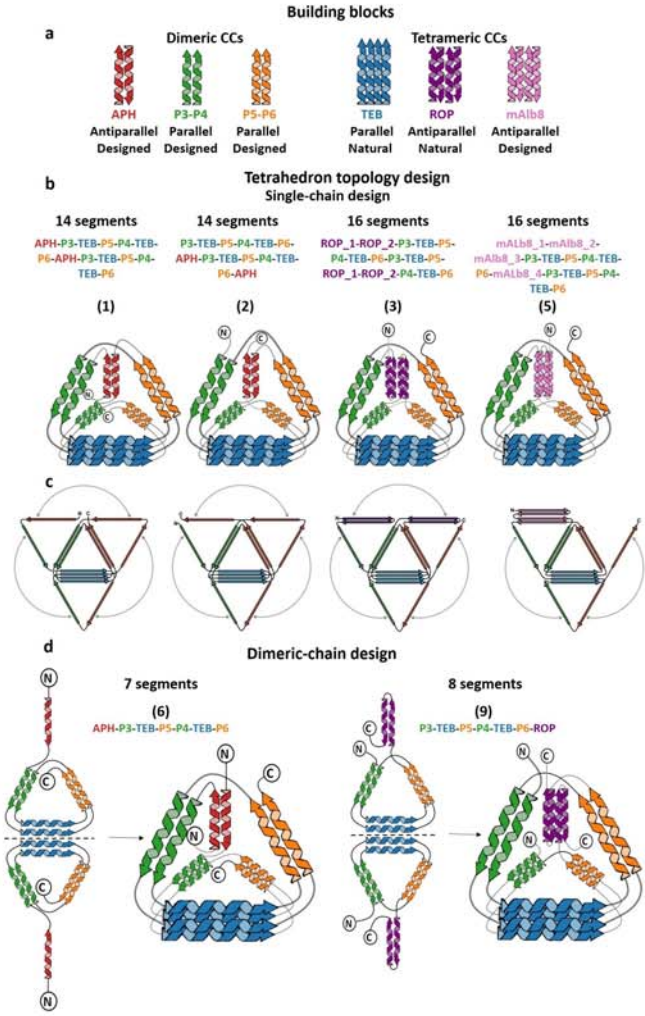

Scheme 1. Coiled-coil building blocks and topologies of designed protein cages composed of a single or two polypeptide chains. a) Building blocks. b) Designed topologies with coiled-coils module sequence and designed fold. c) Two-dimensional representation of folding topologies in b). d) Dimeric-chain designs with peptide sequences and designed fold.

Results and Discussion

Design and Construction

Introducing a tetrameric CC module offers new topological options for the polypeptide chain. However, it also introduces new constraints, as the polypeptide chain has to pass the selected edge four times in the case of a tetramer. Hence, fourteen segments are required to build a tetrahedral nanostructure with a single four-helix bundle: four for the parallel tetrameric segment, eight for the four parallel dimeric CCs, and two for the single antiparallel dimeric CC. We realized that we could further reduce the number of orthogonal building modules to two types of parallel and one antiparallel coiled-coil dimer. For the parallel dimeric modules, we selected two heterodimeric pairs (P3–P4 and P5–P6) designed, characterized, and used in previous studies.[6,7,20–24] Among the sets of antiparallel homodimeric building blocks in the CC toolbox, we opted for the APH[25] module, which shows high stability.[26] The chosen modules enable two different permutations of the polypeptide sequence, designed to fold into the tetrahedral shape (Scheme 1a, b, c). Between each pair of consecutive CC segments, a short flexible peptide linker (GSGPG) was inserted to ensure disruption of the helix and to enable flexibility for vertices of the tetrahedra.[7]

Four helical bundles are composed of peptides with high helical propensity.[27–29] Among the available parallel homotetrameric CC with the desired properties, we identified a right-handed parallel coiled-coil (RHCC) of tetrabrachion (TEB), a surface layer protein from archaea *Staphylothermus marinus*, evolved to survive harsh environmental conditions.[30] The RHCC is part of the stalk domain in TEB and only denatures at extreme conditions such as 1 % (w/v) dodecyl sulfate, 6 M guanidine at 130 °C, or 70 % (w/v) sulfuric acid.[31] For the tetrahedral nanocage, we chose a 52-amino acid residue fragment, which, in contrast to the heptad repeat of the canonical dimeric coiled-coils, has an eleven-residue repeat and folds into a right-handed parallel tetrameric CC.[32] Using this set of building blocks, we created molecular models of the novel proteins in the

Coiled-Coil Protein Origami Design platform (CoCoPOD[6]), which we expanded to include topologies provided by tetrameric modules. We then used it to confirm that the designed sequence could properly fold into tetrahedra-shaped nanocages as the machine learning (ML)-based structure prediction algorithms such as AlphaFold[33] are not yet able to predict the structures of such complex and unnatural topology.

Monomeric Structures

In addition to the full-length sequence of the homotetrameric peptides from tetrabrachion, we tested a shortened version (37 residues long) truncated at the N-terminus (noted as T). The total size of tetrabrachion tetrameric CC spans around 7 nm and 5 nm for the truncated version. Hence, omitting the first 15 residues results in a tetrameric CC that fits better to the length of the other dimeric coiled coils.[6]

Four proteins, designed to form a tetrahedral cage with a single tetrameric module were designed, expressed in *E. coli*, and purified. Tables with annotated sequences are presented in the Supporting Information (Table S1–S3). Based on size-exclusion chromatography, we isolated all proteins in a monodisperse state with a high yield from soluble fractions. We confirmed their expected mass by size-exclusion chromatography coupled with multi-angle light scattering (SEC-MALS) analysis and SDS-PAGE (Figure 1, Figure S1, S2). Circular dichroism (CD) spectra at 25 °C revealed high helical content (Figure 1c, Figure S2), and thermal unfolding experiments showed high stability of the tetrahedral proteins up to 10–20 °C higher compared to previous topologies built solely of dimeric coiled coils[6] (Figure 1 and Figure S2). Cooling back to 25 °C and measuring CD spectra confirmed that all proteins have excellent refolding properties even after heating to high temperatures (up to 95 °C, CD spectra at 95 °C in Figure S2). The hydrodynamic diameter, determined by dynamic light scattering (DLS) before and after heating, confirmed efficient refolding to their initial D_H of 8–9 nm (Figure 1d, Figure S2). However, no significant difference between the hydrodynamic diameter of proteins with a full-length and truncated version of tetrameric CC incorporated was observed by DLS.

Although we have recently published a crystal structure of a CCPO trigon,[34] we were not able to determine the structure of any tetrahedral cage using crystallization or cryo-electron microscopy. We suspected that the failure to obtain good cryogenic samples and cryo-EM structures of CCPOs may be due to their unfolding at the air–water interface (AWI). To check if the incorporation of tetrameric CCs improves resistance to AWI denaturation, we designed an experiment with Nile red dye, which has been used as a sensitive probe for detecting hydrophobic exposed surface in solution that occurs by AWI denaturation.[35,36] First, proteins were mixed with Nile red and measured the fluorescence. Subsequently, the samples were exposed to the AWI by agitation and measured the fluorescence again

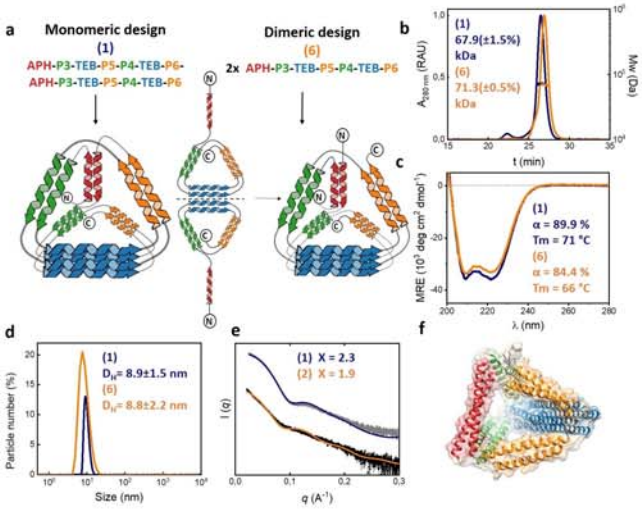

Figure 1. Design and characterization of single-chain and dimeric tetrahedral nanostructures with tetrameric CCs incorporated. a) Protein sequence with 14 or 7 segments fold into tetrahedral nanostructure as a single-chain or dimeric polypeptide, respectively. b) SEC-MALS chromatograms and molecular mass for the (1) (purple line) and its corresponding dimeric protein (6) (orange line). Theoretical MW (1) = 69.0 kDa and MW (6) = 71.0 kDa. UV signal is reported in relative absorbance units (RAU). c) CD spectra of (1) (purple line) and (6) (orange line) at 25 °C with helical content and melting temperature in the panel. d) Hydrodynamic diameter of (1) (purple line) and (6) (orange line) determined by DLS. e) Experimental fit to the SAXS curve of (1) and its corresponding molecular model in f) obtained from the CoCoPOD platform.

(Figure S3a). The proteins with only dimeric CCs exhibited a fluorescence increase after exposure to the AWI, indicating high exposure of hydrophobic regions. In contrast, the proteins compromising a tetrameric coiled coil module showed a significantly lower increase in fluorescence, demonstrating superior resistance to AWI-mediated denaturation. To further confirm this difference, we measured DLS before and after exposure to the air–water interface (Figure S3b). DLS showed that dimeric coiled-coil designs formed larger aggregates after the AWI exposure, indicative of structural destabilization and nonspecific aggregation. In contrast, the tetramer-containing proteins maintained a consistent size distribution, with no significant increase in aggregate formation, highlighting their enhanced stability and resistance to the AWI, suggesting that they may be amenable to cryoEM structure determination.

Structural Characterisation

To confirm the tetrahedral shape of designed cages, we measured SAXS spectra of the isolated proteins in the solution. The molecular models were fit to the experimental curves confirming the tetrahedral nanocage shape for all designs (Figure 1e, Figure S4). All models generated by CoCoPOD displayed a good fit with the experimental data, with χ values in the range of 1.1–2.7. Normalized Kratky plots furthermore confirmed that the proteins are struc-

tured, while the Porod exponents indicated the presence of mobile regions assigned to flexible linkers in the vertices (Figure S4).

To investigate the structural stability and dynamics of the designed proteins, we performed molecular dynamics (MD) simulations to evaluate the effect of introducing a four-helix bundle (4HB) and the new topology. Root-mean-square deviation (RMSD) of the entire tetrahedral cage, separate coiled-coil edges, and linkers were calculated and plotted for the initial structural models and during the whole simulation time (Figure 2, Figure S5). The RMSD of the cage reached the equilibrium state after 50 ns at ~9 Å, which means that the cage stabilized quickly during the simulation. To assess the contribution of the edges and vertices on the overall stability of the cage, we calculated the RMSDs of the six edges and linkers that comprise the four vertices (Figure 2, Figure S5). The values of the six edges are statistically lower than the linkers ($P < 0.001$), suggesting that their truncation could increase the overall rigidity. We also compared the stability of six pairs of edges, which revealed that among the coiled-coil dimer edges, 4HB shows the lowest RMSD value (P value < 0.001), thus indicating higher stability during the simulation and possible stabilization of the rest of the structure as four other segments are anchored to it (Figure 2, Figure S5).

We furthermore analyzed the stability of the four vertices by MD, revealing that the vertices composed of the linkers L1, L4, and L7 have greater flexibility (Figure S5)

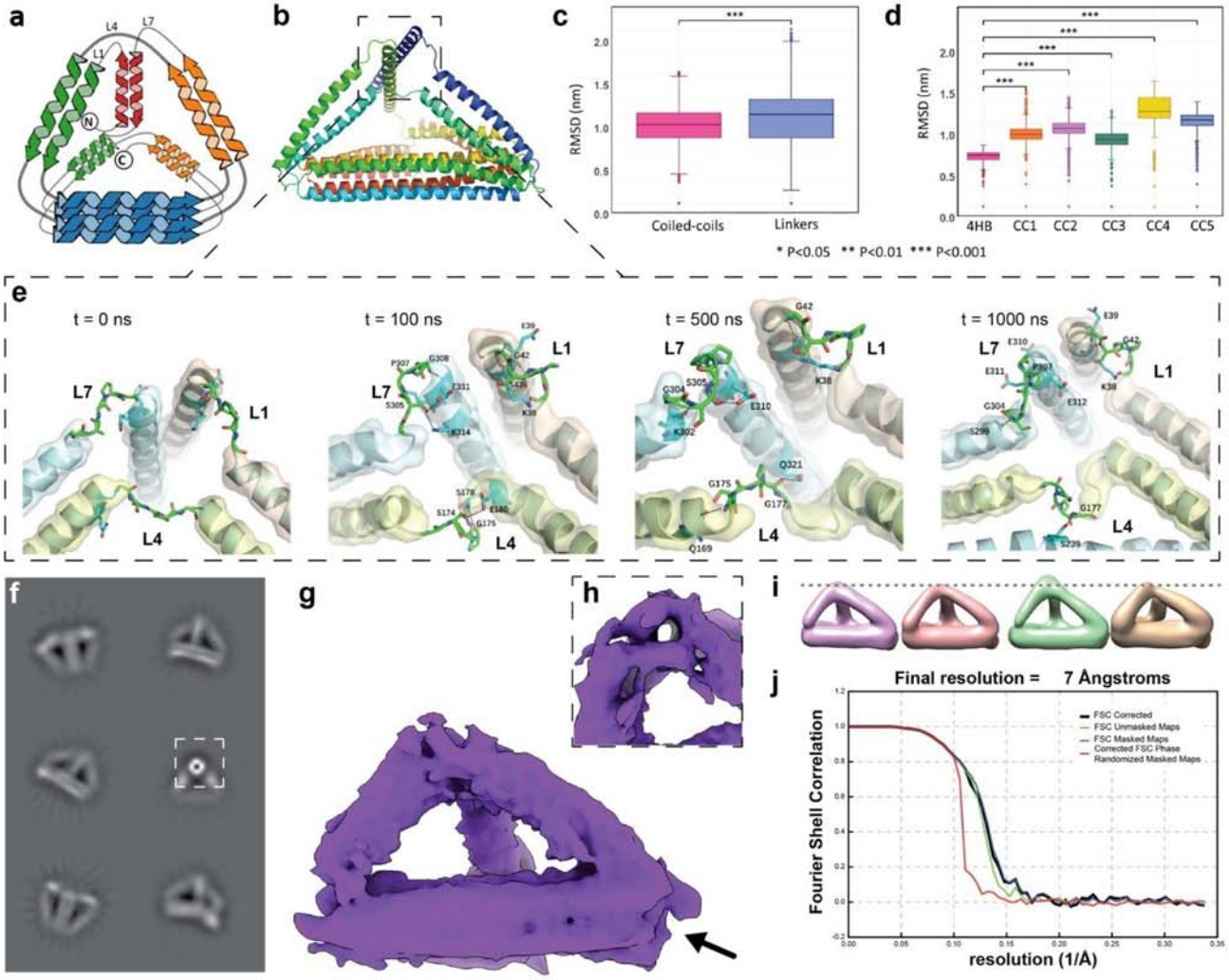

Figure 2. MD simulations of (1) and its structural analysis by cryo-EM. **a)** Schematic representation of the polypeptide path forming a tetrahedron. **b)** Computational model of the tetrahedron cage is composed by a single-chain peptide with 5 dimeric peptide segments and 1 tetrameric module. **c)** Comparison of RMSDs between coiled-coil modules and the linkers. **d)** Comparison of RMSDs between the six coiled-coil modules. **e)** Snapshots (t = 0/100/500/1000 ns, from left to right) of the L1/L4/L7 from 1000 ns MD simulation. Residues from coiled coils and linkers are represented by cyan and green sticks, respectively. Hydrogen bonds are shown as black dashes. **f)** 2D class averages showing the tetrameric module (boxed region) well resolved. **g)** Consensus map reconstruction. **h)** zoom-in on 4HB (viewing direction arrow in g). **i)** 3D variational analysis shows conformational variability around the top vertex (same orientation as in b; dotted gray line for height comparison). **j)** Fourier Shell Correlation (FSC) of the consensus map reconstruction.

and prompting us to observe their conformational changes in four separate simulation snapshots (spaced 500 ns apart). We found that the 1st and 7th linkers maintain hydrogen bonds with the linked coiled-coil terminal residues, while the 4th linker exhibits a more pronounced conformational change. In the snapshot at 500 ns, L4 leaves the vertex position and bends to the edge formed by the 2nd and 8th coiled coil. Additionally, G177 of the linker L4 forms a hydrogen bond with Q321 of the 8th coiled coil. During 550–1000 ns of the simulation, the linker L4 bends to the 4HB edge, and the S166 and G177 residues interact with S239 on the 6th coiled coil to form an unstable hydrogen bond (Figure 2). Overall, the 4HB edge exhibits higher stability than the other edges and significantly contributes to the rigidity of the cage.

To further characterize our tetrahedral designs, we analyzed the single-chain (1) using cryo-electron microscopy and single particle analysis (SPA). 2D classification showed particles in general agreement with the tetrahedral structure. However, except for the four-helix bundle (boxed region Figure 2f), individual helices could not fully be resolved.

To analyze this further, we performed a full 3D reconstruction (Figure 2g, h) and 3D variability analysis (3DVAR). With ca. 13 nm along the longest direction, the dimensions of the particles agree well with the DLS measurements. As predicted, the 4HB segment is structured and allows aligning the designed cage with the atomic model. The other CC edges, however, are less well resolved and the 3DVAR shows movement around the top vertex (Figure 2i), which agrees with the MD simulation. Combined, this flexibility limits the resolution of the final reconstruction (Figure 2j) and prompts further development. Cryo-EM data in (Figure S6).

The existence of a knot has been previously shown in a triangular CCPO,[34] which exemplifies how modular assembly can lead to complex topologies. The presence of a knot, while not predicted by structure prediction tools, highlights the potential alternative topological states, influenced by linker flexibility. These factors may have contributed to the difficulty in high resolution crystal and cryo-EM structure determination.

Designs with Two Tetrameric Coiled-Coils

In a previous report, we used the modular design platform to construct a bipyramid from two polypeptide chains that upon equimolar mixing yielded a bipyramidal nanostructure.[8] The single-chain designs directly repeat the modules after the P6 and APH segments in (1) and (2), respectively (Table S1). Therefore, we reasoned that the two polypeptide chains could self-assemble and form a tetrameric CC even if there are only two repeats of the homotetrameric CC within each chain.[37] To explore this idea, we prepared a series of designs (6, 7, 13, 14). To construct tetrahedra from dimeric symmetric modules and check their folding patterns, we upgraded CoCoPOD for generating protein models from multiple chains. One polypeptide unit could fold into a triangular shape with an unpaired APH helix protruding from the vertex opposite the TEB half-edge. When the tetrameric TEB forms the edge, two APH helices should come together in an antiparallel orientation, to close a tetrahedral nanocage (Scheme 1c, d).

The designed dimerizing proteins were produced and isolated to validate them experimentally. SEC-MALS revealed that the obtained complexes are dimeric in solution (Figure 1, Figure S2). Under the denaturing conditions of SDS PAGE, the interactions between dimers are disrupted, resulting in a single band that corresponds to the molecular weight of the monomer sequence. In comparison, on a native gel, we can only observe a band that corresponds to the size of a dimeric complex (Figure S1, Figure S2). We furthermore confirmed the folding of the dimeric assemblies in agreement with the designs by SAXS analysis, which fits the tetrahedral models constructed in CoCoPOD (Figure 1, Figure S4). The dimeric assemblies showed properties similar to their monomeric congeners, such as high helical content, excellent thermal refolding, and constant hydrodynamic diameter after thermal cycling (Figure 1, Figure S2).

Introducing New Tetrameric Coiled-Coils

Since the homodimeric design allows modifications at symmetric positions within the nanocage, we sought to expand the tetrahedral design further by introducing an additional tetrameric CC to replace the antiparallel APH coiled-coil dimer. However, to introduce a new tetrameric coiled-coil into the existing sequence, it needs to be extended by two additional segments, thus yielding a single chain composed of 16 segments. Furthermore, placing a tetrameric CC at the APH position requires that it folds in an antiparallel fashion. The orientation of the interacting APH dimer was therefore replaced with a heterotetrameric antiparallel CC, and we found that the designed tetrameric coiled-coil mAlb8 meets the criteria.[38]

Two topologies were designed and tested: one in which a tetramer is split into two segments of two helices from mAlb8 (noted as 4) and the other in which mAlb8 is divided into three plus one helices (noted as 5). Again, both single-chain constructs were produced in *E. coli*, purified, and characterized. Their mass was confirmed by SEC-MALS (Figure 3, Figure S2), SDS, and native-PAGE (Figure S1). CD spectra showed that also these proteins have a high helical content and excellent thermal stability accompanied by efficient refolding properties (Figure 3, Figure S2). DLS showed that the hydrodynamic diameter was around 8 nm even after heating and cooling back to room temperature (Figure 3, Figure S2). Molecular models of the two new designs prepared by CoCoPOD exhibited excellent fit to the experimental SAXS curves, confirming that both proteins adopt a tetrahedral nanocage structure (Figure 3, Figure S4).

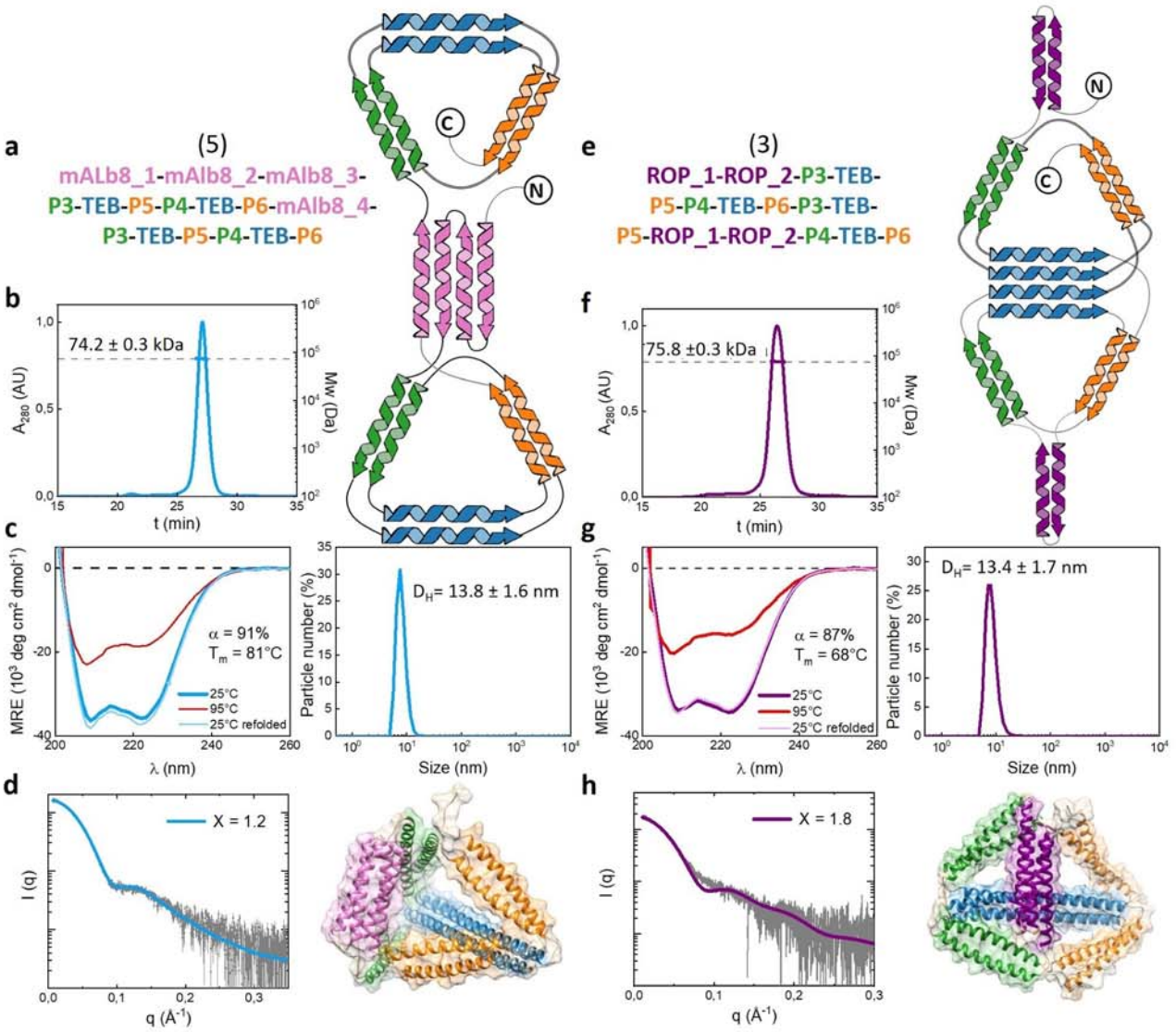

Figure 3. Design and characterization of single-chain tetrahedral topologies with incorporated two pairs of tetrameric CCs. a) segment sequence of single-chain tetrahedra (5) and its 2D topological scheme on the right with TEB tetramer presented as unpaired dimers. b) SEC-MALS chromatogram and molecular mass for the (5). Theoretical Mw (5) = 74.4 kDa. UV signal is reported in relative absorbance units (AU). c) CD spectra of the protein at 25 °C, 95 °C and cooled back to 25 °C showing excellent refolding properties with helical content percentage and the melting temperature indicated within the panel on the left. The hydrodynamic diameter of the protein is determined by DLS on the right. d) The experimental SAXS profile of the (5) (gray trace) matching well the theoretical SAXS profile calculated for the protein model structure ($\chi = 1.2$) (blue line). Error bars in gray represent the standard deviation for each data point (mean). Molecular model corresponding to fit curve obtained in CoCoPOD platform on the right. e) Segment sequence of single-chain tetrahedra (3) and its 2D topological scheme on the right with ROP tetramer presented as unpaired dimers. f) SEC-MALS chromatogram and molecular mass for the (3). Theoretical Mw (3) = 74.7 kDa. UV signal is reported in relative absorbance units (AU). g) CD spectra of the protein at 25 °C, 95 °C and cooled back to 25 °C showing excellent refolding properties with helical content percentage and the melting temperature indicated within the panel, on the left. The hydrodynamic diameter of the protein determined by DLS is shown on the right. h) The experimental SAXS profile of the (3) (gray trace) matching well with the theoretical SAXS profile calculated for the protein model structure ($\chi = 1.8$) (purple trace). Error bars in black represent the standard deviation for each data point in black (mean). The molecular model corresponding fitting the SAXS curve obtained in the CoCoPOD platform on the right.

Dimeric Designs

We next constructed a dimeric tetrahedral nanocage based on an additional four helical bundle segment. However, the hetero-tetrameric mAlb8 module cannot be used for such designs as it requires that the two joining segments are homomeric and in an antiparallel orientation, as in APH. We found that the naturally occurring repressor of primer (ROP) meets this criterion. ROP is a small dimeric RNA-binding protein that comprises a four-helix bundle with a regular heptad motif.[39,40]

We thus constructed a dimeric self-assembling tetrahedral nanocage with the corresponding order of segments as in (6) and (7) but using the antiparallel ROP dimer to

replace the APH position. The protein sequence thus comprises eight segments, resulting in the proteins (8) and (9). Similar to before, the two new protein variants were designed and isolated in high yield as monomeric proteins on SDS, analogous to the APH-containing dimeric proteins. Their tetrahedral shape in solution was confirmed by fitting the experimental SAXS curves to the molecular models (Figure S4). Both proteins showed high helical content and excellent refolding properties after thermal unfolding (Figure S2). The hydrodynamic diameter was comparable to the APH analogs (Figure S2).

To test the full set of permutations, we sought to also incorporate ROP into the single-chain tetrahedral fold. However, the segment could not follow the sequence of (1) due to the complexity of the antiparallel orientation in the ROP dimer. Instead, it could be constructed according to the topology of (4). Therefore, we introduced ROP into this design, produced, and isolated the new protein (3). The characterization revealed a stable and highly helical protein and the fit of molecular models to experimental SAXS scattering curves confirmed the tetrahedral shape (Figure 3h). With this study, we have expanded the range of CCPO topologies by introducing four-helix bundle modules, which allow the construction of symmetric assemblies and symmetric functionalization.

Conclusions

Protein design has recently been streamlined by the application of generative machine learning.[33,41–44] Modular design principles, on the other hand, have several unique advantages, as we can select the building blocks for stability,[45] pH[46] or metal ion-based regulation,[47] conformational oligomerization switches,[48] or chemical reaction sites.[49] Here, we present an extension of the modular design strategy by introducing tetrameric coiled coils. Seven new structures comprising new topological folds were designed that exhibited high stability and excellent refolding properties. Importantly, we show that designs that comprise four-helix bundles are more resistant to air–water interface denaturation, most likely due to the high stability of this segment as it is highly entangled with other segments of the cage and also most rigid as assessed from MD simulation. The tetrahedral nanocage shape was confirmed by SAXS for all proteins, highlighting the robust folding into the desired shapes despite the flexible linkers used. A high-resolution structure of the trigonal CCPO protein has been recently determined by X-ray, which required optimization of the length of linkers and CC edges.[34] We now present the first tetrahedral protein cage characterized by cryo-EM confirming the correct assembly also in the solution. Selection of short linkers and more stable CC modules might help to improve the structural definition as recently demonstrated by a high-resolution structure of a CCPO trigon comprising only CC dimers.[34]

In addition to the novel single-chain designs containing a tetramerization module, we present proteins that assemble from two identical units, which in the case of only CC-dimer modules required cyclization.[9] The introduction of tetrameric modules demonstrates and expands the flexibility of the CCPO design platform. The dimeric strategy opens up avenues for functionalization at symmetric positions within the monomeric and the smallest symmetric dimeric designs. External modulators, such as proteases,[8] metal ions,[50] pH, and many other triggers may be used to regulate the assembly state. It is likely that other oligomeric states could be used to introduce new modular biomolecular nanostructures with new features.

Acknowledgements

This research was supported by a complementary MSCA scheme grant (N1-0125) from the Ministry of Higher Education, Science and Innovation of Slovenia from the Slovenian Research Agency and projects P4-0186, N1-0377, J1-2481, J1-4406, N1-0323 and received funding from the European Research Council (ERC) under the European Union's Horizon 2020 research, innovation program Advanced Grant project MaCChines Grant agreement ID: 899259, EU FET Open Project Virofight (#899619) and CZI CryoCLEM Grant (awarded to PSE and RJ). We thank Jürgen Plitzko for the microscope access, and Sven Klumpe for help with the data modelling.

Conflict of Interest

The authors declare no conflict of interest.

Data Availability Statement

The data that support the findings of this study are available in the supplementary material of this article.

Keywords: coiled-coils · protein origami · cryo-electron microscopy · protein design

[1] N. C. Seeman, *Mol. Biotechnol.* **2007**, *37*, 246–257.
[2] S. Woo, P. W. K. Rothemund, *Nat. Chem.* **2011**, *3*, 620–627.
[3] K. F. Wagenbauer, C. Sigl, H. Dietz, *Nature* **2017**, *552*, 78–83.
[4] H. Dietz, S. M. Douglas, W. M. Shih, *Science.* **2009**, *325*, 725–730.
[5] F. Ricci, H. Dietz, *Nat. Nanotechnol.* **2023**, *18*, 541–542.
[6] A. Ljubetič, F. Lapenta, H. Gradišar, I. Drobnak, J. Aupič, Ž. Strmšek, D. Lainšček, I. Hafner-Bratkovič, A. Majerle, N. Krivec, M. Benčina, T. Pisanski, T. Ć. Veličković, A. Round, J. M. Carazo, R. Melero, R. Jerala, *Nat. Biotechnol.* **2017**, *35*, 1094–1101.
[7] H. Gradišar, S. Božič, T. Doles, D. Vengust, I. Hafner-Bratkovič, A. Mertelj, B. Webb, A. Šali, S. Klavžar, R. Jerala, *Nat. Chem. Biol.* **2013**, *9*, 362–366.
[8] F. Lapenta, J. Aupič, M. Vezzoli, Ž. Strmšek, S. Da Vela, D. I. Svergun, J. M. Carazo, R. Melero, R. Jerala, *Nat. Commun.* **2021**, *12*, 939.
[9] J. Snoj, F. Lapenta, R. Jerala, *Chem. Sci.* **2024**, *15*, 3673–3686.

[10] B. Apostolovic, M. Danial, H. A. Klok, *Chem. Soc. Rev.* **2010**, *39*, 3541–3575.
[11] P. Burkhard, J. Stetefeld, S. V. Strelkov, *Trends Cell Biol.* **2001**, *11*, 82–88.
[12] D. N. Woolfson, *Subcell. Biochem.* **2017**, *82*, 35–61.
[13] L. Truebestein, T. A. Leonard, *BioEssays* **2016**, *38*, 903–916.
[14] J. Aupič, Ž. Strmšek, F. Lapenta, D. Pahovnik, T. Pisanski, I. Drobnak, A. Ljubetič, R. Jerala, *Nat. Commun.* **2021**, *12*, 940.
[15] A. D. Malay, N. Miyazaki, A. Biela, S. Chakraborti, K. Majsterkiewicz, I. Stupka, C. S. Kaplan, A. Kowalczyk, B. M. A. G. Piette, G. K. A. Hochberg, D. Wu, P. Wrobel, A. Fineberg, M. S. Kushwah, M. Kelemen, P. Vavpetič, P. Pelicon, P. Kukura, J. L. P. Benesch, K. Iwasaki, J. G. Heddle, *Nature* **2019**, *569*, 438–442.
[16] K. A. Cannon, V. N. Nguyen, C. Morgan, T. O. Yeates, *ACS Synth. Biol.* **2020**, *2020*, 517–524.
[17] E. Golub, R. H. Subramanian, J. Esselborn, R. G. Alberstein, J. B. Bailey, J. A. Chiong, X. Yan, T. Booth, T. S. Baker, F. A. Tezcan, *Nature* **2020**, *578*, 172–176.
[18] J. Jorda, D. J. Leibly, M. C. Thompson, T. O. Yeates, *Chem. Commun.* **2016**, *52*, 5041–5044.
[19] S. A. McConnell, K. A. Cannon, C. Morgan, R. McAllister, B. R. Amer, R. T. Clubb, T. O. Yeates, *ACS Synth. Biol.* **2020**, *9*, 381–391.
[20] H. Gradišar, R. Jerala, *J. Pept. Sci.* **2011**, *17*, 100–106.
[21] I. Drobnak, H. Gradišar, A. Ljubetič, E. Merljak, R. Jerala, *J. Am. Chem. Soc.* **2017**, *139*, 8229–8236.
[22] T. Lebar, D. Lainšček, E. Merljak, J. Aupič, R. Jerala, *Nature* **2020**, *16*, 513–519.
[23] T. Fink, J. Lonzarić, A. Praznik, T. Plaper, E. Merljak, K. Leben, N. Jerala, T. Lebar, Ž. Strmšek, F. Lapenta, M. Benčina, R. Jerala, *Nat. Chem. Biol.* **2019**, *15*, 115–122.
[24] D. Lainšček, V. Forstnerič, V. Mikolič, Š. Malenšek, P. Pečan, M. Benčina, M. Sever, H. Podgornik, R. Jerala, *Nat. Commun.* **2022**, *13*, 3604.
[25] D. G. Gurnon, J. A. Whitaker, M. G. Oakley, *J. Am. Chem. Soc.* **2003**, *125*, 7518–7519.
[26] C. Negron, A. E. Keating, *J. Am. Chem. Soc.* **2014**, *136*, 16544–16556.
[27] S. E. Boyken, Z. Chen, B. Groves, R. A. Langan, G. Oberdorfer, A. Ford, J. Gilmore, C. Xu, F. Dimaio, J. H. Pereira, B. Sankaran, G. Seelig, P. H. Zwart, D. Baker, *Science.* **2016**, *352*, 680–687.
[28] E. Merljak, B. Malovrh, R. Jerala, *Nat. Commun.* **2023**, *14*, 1995.
[29] Z. Chen, S. E. Boyken, M. Jia, F. Busch, D. Flores-Solis, M. J. Bick, P. Lu, Z. L. Vanaernum, A. Sahasrabuddhe, R. A. Langan, S. Bermeo, J. Brunette, V. K. Mulligan, L. P. Carter, F. Dimaio, N. G. Sgourakis, V. H. Wysocki, D. Baker, *Nature* **2019**, *565*, 106–111.
[30] J. Peters, M. Nitsch, B. Kühlmorgen, R. Golbik, A. Lupas, J. Kellermann, H. Engelhardt, J.-P. Pfander, S. Müller, K. Goldie, A. Engel, K.-O. Stetter, W. Baumeister, *J. Mol. Biol.* **1995**, *245*, 385–401.
[31] J. Peters, W. Baumeister, A. Lupas, *J. Mol. Biol.* **1996**, *257*, 1031–1041.
[32] J. Stetefeld, M. Jenny, T. Schulthess, R. Landwehr, J. Engel, R. A. Kammerer, *Nat. Struct. Biol.* **2000**, *7*, 772–776.
[33] J. Jumper, R. Evans, A. Pritzel, T. Green, M. Figurnov, O. Ronneberger, K. Tunyasuvunakool, R. Bates, A. Žídek, A. Potapenko, A. Bridgland, C. Meyer, S. A. A. Kohl, A. J. Ballard, A. Cowie, B. Romera-Paredes, S. Nikolov, R. Jain, J. Adler, T. Back, S. Petersen, D. Reiman, E. Clancy, M. Zielinski, M. Steinegger, M. Pacholska, T. Berghammer, S. Bodenstein, D. Silver, O. Vinyals, A. W. Senior, K. Kavukcuoglu, P. Kohli, D. Hassabis, *Nature* **2021**, *596*, 583–589.
[34] T. Satler, S. Hadži, R. Jerala, *J. Am. Chem. Soc.* **2023**, *145*, 16995–17000.
[35] D. L. Leiske, I. C. Shieh, M. L. Tse, *Langmuir* **2016**, *32*, 9930–9937.
[36] M. Sutter, S. Oliveira, N. N. Sanders, B. Lucas, A. Van Hoek, M. A. Hink, A. J. W. G. Visser, S. C. De Smedt, W. E. Hennink, W. Jiskoot, *J. Fluoresc.* **2007**, *17*, 181.
[37] V. A. Streltsov, P. M. Schmidta, J. L. M. K. Breschkina, *Acta Crystallogr. Sect. F Struct. Biol. Commun.* **2019**, *75*, 89–97.
[38] A. Baryshev, A. La Fleur, B. Groves, C. Michel, D. Baker, A. Ljubetič, G. Seelig, *Nat. Chem. Biol.* **2024**, *20*, 1514–1523.
[39] M. Vlassi, C. Steif, P. Weber, D. Tsernoglou, K. S. Wilson, H. J. Hinz, M. Kokkinidis, *Nat. Struct. Biol.* **1994**, *1*, 706–716.
[40] M. A. Willis, B. Bishop, L. Regan, A. T. Brunger, *Structure* **2000**, *8*, 1319–1328.
[41] Z. Chen, M. C. Johnson, J. Chen, M. J. Bick, S. E. Boyken, B. Lin, J. J. De Yoreo, J. M. Kollman, D. Baker, F. DiMaio, *J. Am. Chem. Soc.* **2019**, *141*, 8891–8895.
[42] J. L. Watson, D. Juergens, N. R. Bennett, B. L. Trippe, J. Yim, H. E. Eisenach, W. Ahern, A. J. Borst, R. J. Ragotte, L. F. Milles, B. I. M. Wicky, N. Hanikel, S. J. Pellock, A. Courbet, W. Sheffler, J. Wang, P. Venkatesh, I. Sappington, S. Vázquez Torres, A. Lauko, V. De Bortoli, E. Mathieu, S. Ovchinnikov, R. Barzilay, T. S. Jaakkola, F. DiMaio, M. Baek, D. Baker, *Nature* **2023**, *620*, 1089–1100.
[43] J. Dauparas, I. Anishchenko, N. Bennett, H. Bai, R. J. Ragotte, L. F. Milles, B. I. M. Wicky, A. Courbet, R. J. de Haas, N. Bethel, P. J. Y. Leung, T. F. Huddy, S. Pellock, D. Tischer, F. Chan, B. Koepnick, H. Nguyen, A. Kang, B. Sankaran, A. K. Bera, N. P. King, D. Baker, *Science.* **2022**, *378*, 49–56.
[44] P. S. Huang, S. E. Boyken, D. Baker, *Nature* **2016**, *537*, 320–327.
[45] W. Bai, C. J. Sargent, J.-M. Choi, R. V. Pappu, F. Zhang, *Nat. Commun.* **2019**, *10*, 3317.
[46] R. Lizatović, O. Aurelius, O. Stenström, T. Drakenberg, M. Akke, D. T. Logan, I. André, *Structure* **2016**, *24*, 946–955.
[47] J. Aupič, F. Lapenta, R. Jerala, *ChemBioChem* **2018**, *19*, 2453–2457.
[48] J. Liu, Q. Zheng, Y. Deng, N. R. Kallenbach, M. Lu, *J. Mol. Biol.* **2006**, *361*, 168–179.
[49] W. Mathis Rink, F. Thomas, *Chem. A Eur. J.* **2019**, *25*, 1665–1677.
[50] J. Aupič, F. Lapenta, Ž. Strmšek, E. Merljak, T. Plaper, R. Jerala, *Sci. Adv.* **2022**, *8*, 8243.

Manuscript received: November 13, 2024
Accepted manuscript online: December 12, 2024
Version of record online: December 20, 2024